Modeling divertor concepts for spherical tokamaks NSTX-U and ST-FNSF

E.T. Meier[1], V.A. Soukhanovskii[1], R.E. Bell[2], A. Diallo[2], S. Gerhardt[2], R. Kaita[2], B.P. LeBlanc[2], A.W. Leonard[3], A.G. McLean[1], J.E. Menard[2], M. Podesta[2], T.D. Rognlien[1] and F. Scotti[1]

[1]Lawrence Livermore National Laboratory, Livermore, CA 94551, USA
[2]Princeton Plasma Physics Laboratory, P.O. Box 451, Princeton, NJ 08543, USA
[3]General Atomics, P.O. Box 85608, San Diego, CA 92186, USA

Corresponding Author: meier23@llnl.gov

Abstract:
The compact nature of the spherical tokamak (ST) presents an economically attractive path to fusion commercialization, but concentrates power exhaust, threatening the integrity of plasma-facing components. To address this challenge, experimentally constrained divertor modeling in the National Spherical Torus Experiment (NSTX) is extrapolated to investigate divertor concepts for future ST devices. Analysis of NSTX Upgrade with UEDGE shows that the secondary snowflake X-point position can be adjusted for favorable neutral transport, enabling stable partial detachment at reduced core densities. For a notional ST-based Fusion Nuclear Science Facility, divertor concepts are identified that provide heat flux mitigation (<10 MW/m^2) and low temperatures (<10 eV) compatible with high-Z targets. This research provides guidance for upcoming experiments and a basis for continued development of predictive capability for divertor performance in STs.

1 Introduction

As fusion research progresses toward the reactor scale, increasingly intense power exhaust threatens the integrity of plasma facing components. The compact nature, i.e., small major radius (R), of the spherical tokamak (ST) presents an economically attractive path to fusion commercialization [1], but magnifies the power exhaust challenge, because the plasma-wetted area is proportional to R. Addressing this challenge, heat flux mitigation techniques, focusing on the snowflake divertor (SFD) configuration [2] and the effects of target tilt, have been considered for two future STs: the National Spherical Torus eXperiment Upgrade (NSTX-U) [3], and a notional ST-based Fusion Nuclear Science Facility (ST-FNSF) [1].

Many heat flux mitigation techniques aim to induce detachment of the scrape-off layer (SOL) plasma from the divertor target(s). In detached operation, it is important to stabilize the cold, dense plasma in the divertor, preventing direct interaction with (and excessive cooling of) the core plasma. One way to achieve stable detachment is to detach a limited portion of the near SOL (e.g., within one heat flux width), while the far SOL (beyond one heat flux width) remains attached—this corresponds to the planned partial detachment in ITER [4]. The transition to (partial) detachment can be characterized as a function of upstream density. A relatively low detachment density threshold may help to avoid density-related global stability limits and enable exploration of improved energy confinement expected in STs at low collisionality [3]. In the analysis presented below, detachment stability and transition density will be highlighted.

A multi-fluid edge transport code, UEDGE [5, 6], has recently been used to analyze the SFD heat flux mitigation technique pioneered on NSTX [7]. Simulations captured the partial detachment observed experimentally in the SFD, reproducing the several-fold reduction of divertor heat flux, and 10-fold increase in divertor D_α brightness, while matching upstream plasma profiles [8]. The UEDGE analysis showed that a combination of factors enabled stable, repeatable detachment in the SFD: 1) enhanced radiation (due to the large divertor volume); 2) power transmission to the targets through the neutral gas channel, which reduced electron temperature (T_e) below 0.5 eV, inducing volumetric recombination; and 3) increased recycling due to saturation of the lithium pumping mechanism. Moreover, by demonstrating the ability of UEDGE to model ST detachment physics, the analysis provided a basis for the divertor concept research presented in this paper.

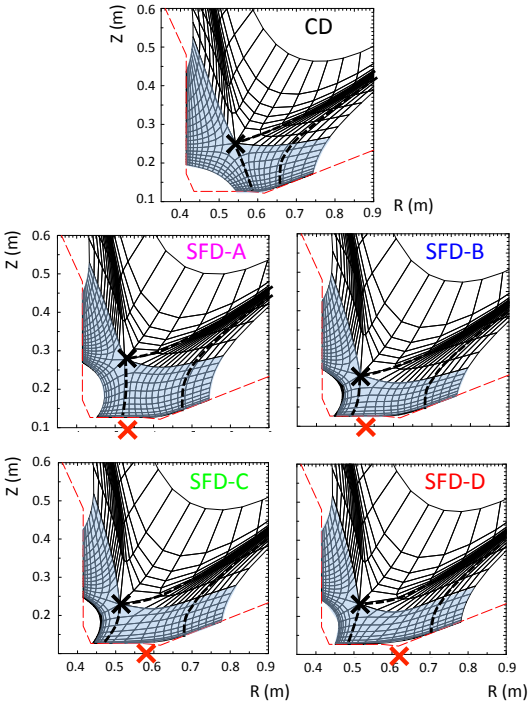

FIG. 1: Divertor region of UEDGE grids for conventional divertor (CD) and snowflake divertor (SFD) simulations of NSTX-U. Primary and secondary (snowflake) X-points are shown with black and red X's, respectively. Dashed lines indicate 3-mm flux tubes. Divertor volumes are indicated with blue shading.

NSTX Upgrade (NSTX-U) will have up to 12 MW neutral beam power and 2 MA plasma current [3]. The expected unmitigated divertor target heat fluxes will be more than twice as high as observed in NSTX [9]. Initial NSTX-U SFD and conventional divertor (CD) configurations presented in [3] have been evaluated with UEDGE [10]. In terms of heat flux reduction and detachment density threshold, limited advantage was seen for the SFD compared to the CD.

Section 2 presents an optimization of the SFD for NSTX-U, building on earlier modeling [8, 10]. Section 3 describes preliminary assessment of divertor concepts for an ST-based Fusion Nuclear Science Facility (ST-FNSF) [1]. Conclusions are drawn in Section 4.

2 NSTX-U modeling

Setup. Computational grids for UEDGE simulations of NSTX-U are based on five lower-single-null equilibria generated with ISOLVER, a free-boundary Grad-Shafranov equilibrium code [11]. The toroidal magnetic field is $B_t = 1$ T at the magnetic axis and the plasma current is $I_p = 2$ MA. Divertor regions of the five grids are shown in Fig. 1. Flux tubes spanning one heat flux width, i.e., 3 mm in the outer midplane (OMP) in these NSTX-U cases [9], clearly show expanded target footprints in the SFD cases. The divertor volume (V_{div}), however, varies little: SFD-A and -B have the largest and smallest volumes, V_{div}=0.19 m^3 and V_{div}=0.15 m^3, respectively. Earlier research [10] studied only the CD and SFD-A. The present work evaluates an additional range of topologies given by SFD-B, -C, and -D, in which the secondary X-point is translated radially outward.

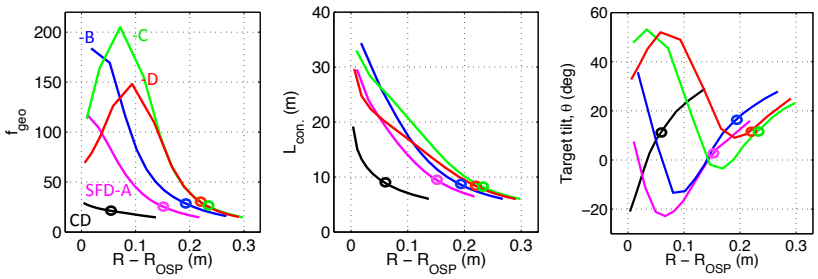

FIG. 2: Magnetic geometries for UEDGE NSTX-U simulations. Geometric flux expansion (f_{geo}), midplane-to-target field line connection length (L_{con}), and "target tilt" are shown as functions of radial position on the outer target with respect to the outer strike point (OSP) for the five configurations considered. Circular markers are placed at radial locations corresponding to 3 mm in the outer midplane.

Magnetic geometries of the SFD configurations are obviously modified with respect to the CD, as seen in Fig. 2, but subtle (and, as will be shown, important) differences exist between the four SFD. Geometric flux expansion is defined as $f_{geo} \equiv f_{exp}/\cos(\theta)$, where f_{exp} is the poloidal flux expansion, and θ is the "target tilt"—the angular deviation from normal incidence of flux surfaces on the target. For SFD-A and -B, f_{geo} peaks near the separatrix, while for SFD-C and -D, the peaks are shifted radially outward. Connection lengths (L_{con}) for the SFD cases are typically 50% greater than for the CD. The plot of θ shows that SFD-C and -D have $\theta > 0$ in most or all of the region corresponding to the 3-mm flux tube. Here, $\theta > 0$ indicates an acute angle between the outboard target and the flux surface. As discussed in detail below, for $\theta > 0$, neutral particles are guided toward the separatrix; for $\theta < 0$, the opposite is true.

At the core-edge interface (CEI), the core density (n_{core}) is fixed for a given simulation (and varied in simulation scans as described below). Power through the CEI, split evenly between ion and electron channels, is 9 MW, corresponding to a high-power NSTX-U scenario. At the high-field-side (i.e., the inner wall), neutral gas is injected at 2.5×10^{21} s^{-1}. Perpendicular thermal transport coefficients for ions and electrons are 2 m^2/s at the CEI, increase (as a cubic function of radius) to 4 m^2/s at the separatrix, and are uniform in the SOL. Similarly, perpendicular particle transport varies from 0.1 m^2/s at the CEI to 0.5 m^2/s at the separatrix and in the SOL. Perpendicular transport is assumed to be poloidally uniform. Target recycling efficiencies of ions and neutrals are 99% and 100%, respectively. At the outer boundary, ion and neutral recycling are 90%. At the private flux region (PFR) boundary, ion recycling is 90%, while neutral recycling is 100%. Carbon impurities are included in the simulation at a fixed 3% concentration.[1] At the outer and PFR boundaries, ion density and temperatures are assigned 2-cm gradient scale lengths. The model for neutral gas power transfer to divertor targets discussed in Ref. [8] (and which proved crucial to accurately modeling detachment) is employed. Plasma drifts are not included.

Results and discussion. Significant variation is found in the detachment behavior of the five divertor configurations. Shown in Fig. 3 are results from a scan of core density (n_{core}) from 2×10^{19} to 4.5×10^{19} m^{-3}, with steps of 0.1×10^{19} m^{-3}. Total divertor ion inventories (N_{div}) for the CD, SFD-A, and -B are similar across the density range, rising slowly then abruptly increasing five-fold at $n_{core} \approx 4.5 \times 10^{19}$ m^{-3}, corresponding to unstable detachment as discussed, e.g., in [12]; experimentally, such sudden detachment onset has recently been observed on the DIII-D

[1] Charge-state-resolved impurity modeling has proven difficult to validate in NSTX modeling [8]; therefore the simpler fixed concentration model is used here.

tokamak [13]. In contrast, N_{div} for SFD-C and -D are significantly higher, and rise more steadily. The Greenwald fraction (f_{GW}) (calculated as $f_{GW} \equiv \bar{n}/n_{GW}$, where $\bar{n}$ is estimated as three times the outer midplane separatrix density, consistent with NSTX data) is similar for all cases, and detachment occurs at values of f_{GW} appropriate for the NSTX-U mission [3]. For SFD-C and -D, $P_{rad,div}$ rises at lower n_{core} than the other cases, and increases gradually as seen in N_{div}. Total power reaching the inner and outer divertor targets (Q_{div}) has a strong inverse correlation with N_{div} and $P_{rad,div}$. At or below 4.7×10^{19} m^{-3}, all configurations exhibit detached conditions across most of the outer and inner targets, and the artificial grid boundaries strongly influence the solutions, apparently preventing complete collapse of the core plasma.

Detachment progresses radially across the outer target in the SFD-D scan of n_{core}, as illustrated in Fig. 4. At $n_{core} = 2 \times 10^{19}$ m^{-3}, a small zone in the PFR has neutral gas density (n_g) higher than the deuterium ion density (n_i). Using the position at which $n_g = n_i$ (i.e., 50% ionization) as a proxy for transition from detached ($n_g > n_i$) to attached ($n_g < n_i$), plots at $n_{core} = 2.8$ and 3.5×10^{19} m^{-3} show that the detached zone spreads from the PFR to a location near 0.12 m on the outer target. Peak heat flux is 5.2 MW/m^2 at $n_{core} = 2.0 \times 10^{19}$ m^{-3}, safely below 10 MW/m^2 (the typical technological limit); however, within the 3-mm flux tube (which extends to $R = 0.21$), T_e (not shown) exceeds 50 eV. At $n_{core} = 3.5 \times 10^{19}$ m^{-3}, peak heat flux is only slightly lower at 4.2 MW/m^2, but T_e is below 10 eV within the 3-mm flux tube; heat flux in that region is dominated by radiation, as shown. Because high target T_e can lead to excessive impurity sputtering and contamination of the upstream SOL, eliminating high target T_e in the near-separatrix region is mandatory to prevent subsequent core impurity buildup. Furthermore, SOL impurity transport analysis shows that high recycling conditions—low T_e and high density—tend to improve impurity retention in the divertor region [14].

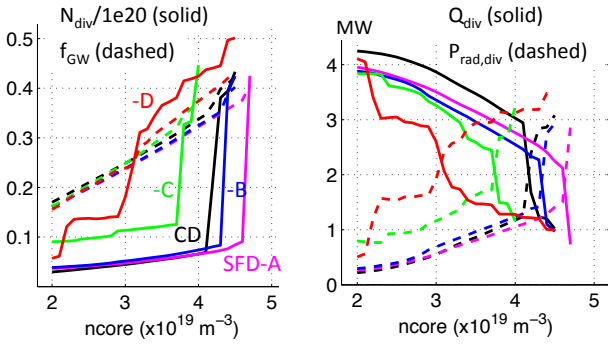

FIG. 3: Results of density scan for NSTX-U configurations. Greenwald fraction (f_{GW}) and the total divertor ion inventory (N_{div}) are plotted as a function of core density (left). Total power reaching the divertor (Q_{div}) and power radiated in the divertor ($P_{rad,div}$) are also shown (right).

Divertor target conditions in SFD-C are qualitatively similar to SFD-D. In SFD-A and -B, peak outer target heat flux is < 6 MW/m^2 across the range of n_{core} studied, but solutions show high temperatures inside the 3-mm flux tube except following sudden detachment at $n_{core} \approx 4.5 \times 10^{19}$ m^{-3}. The CD case has an unacceptable 16 MW/m^2 peak outer target heat flux at $n_{core} = 2 \times 10^{19}$ m^{-3}. Notably, *all* of the five divertor configurations have peak heat flux above 10 MW/m^2 at the inner target at $n_{core} = 2 \times 10^{19}$ m^{-3}, but the inner target heat flux is mitigated to < 10 MW/m^2 for $n_{core} > 2.3 \times 10^{19}$ m^{-3} for all configurations.

These UEDGE results suggest that seemingly subtle changes in secondary X-point location in the SFD can cause dramatic changes in detachment behavior. In SFD-D, for example, the detachment progresses continuously as core density is increased, whereas for SFD-A, detachment occurs abruptly at high core density. The existence of a gradual detachment transition offers operators some margin for error when aiming for partial detachment via, e.g., manual or automatic adjustment of divertor gas puffing or impurity injection; in divertors with abrupt de-

tachment behavior, full detachment and X-point MARFE formation might be difficult to avoid when seeking partially detached states.

The gradual detachment in SFD-D is enabled by neutral transport physics. In UEDGE, the flux of neutral gas particles across flux surfaces (i.e., in the "radial" direction) is given by $\Gamma_{g,r} = n_g v_{g,r}$. The radial neutral velocity is $v_{g,r} = \nabla_r p_g/(m_g n_g f_{xs})$, where m_g is the neutral particle mass, p_g is the neutral pressure, and f_{xs} is the sum of charge exchange and scattering collision frequencies. Ion recycling at targets naturally generates strong normal neutral pressure gradients. Assuming that ∇p_g is dominated by a component normal to the divertor target, $\nabla_r p_g = \nabla p_g \sin(\theta)$. Tangential components of ∇p_g may play a role, but results presented above suggest that "tilt-induced" transport is dominant. SFD-C and -D, have θ up to 50° over the part of the target corresponding to the 3-mm flux tube, and the fact that detachment occurs in those cases at relatively low n_{core} is explained by the effect of target tilt on neutral transport. The gradual progression of detachment as a function of n_{core} in SFD-C and -D can also be understood in terms of tilt-induced transport. As detachment proceeds radially outward across the target, θ in SFD-C and -D is reduced from $\sim 50°$ to $\lesssim 10°$. The reduction of tilt-induced transport partially balances the increased density and radiation that typically occur as a detachment front moves upstream and, in this case, as the detached-to-attached transition point moves radially across the target as in Fig. 4. In [12], such a position-dependent reduction in transport and radiation is identified as a requirement for detachment stability.

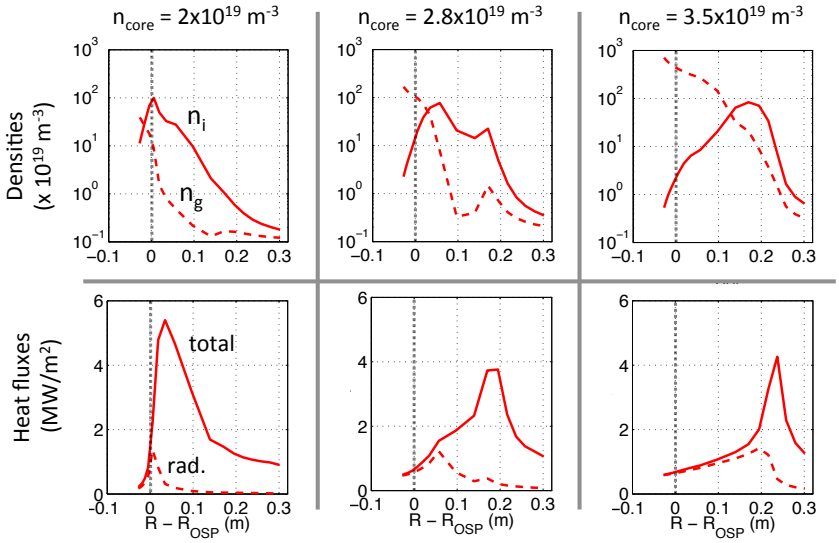

FIG. 4: SFD-D divertor target profiles. Densities (top row) and heat fluxes (bottom row) are shown as a function of radial distance past the outer strike point for three different core densities.

3 ST-FNSF modeling

Setup. Four ST-FNSF divertor configurations are modeled with UEDGE: a conventional divertor (CD); a CD with vertical target (CD-VT); a snowflake divertor (SFD); and a super-SFD, i.e, a SFD with extended outer divertor leg as in the Super-X divertor [15, 16]. Shown in Fig. 5 are computational grids for the four cases, based on up-down symmetric (i.e., balanced double-null) equilibria generated with ISOLVER. $B_t = 2.4$ T at the magnetic axis and $I_p = 12$ MA.

Examining the magnetic geometries, the CD and CD-VT have similar geometric expansion, $f_{geo} \approx 30$ near the OSP. The SFD has significantly more expansion, with $f_{geo} \approx 55$ near the OSP, while the super-SFD has $f_{geo} \approx 8$ near the OSP. Connection lengths are $L_{con} \approx 20$ m near the OSP for both CD and CD-VT cases, and $L_{con} \approx 25$ and 50 m for the SFD and super-SFD,

respectively. The CD and SFD cases have negative "target tilt," $\theta \approx -40°$ across the targets, directing neutrals away from the OSP (see discussion of target tilt in Section 2). In contrast, $\theta \approx 40°$ and 80° across the CD-VT and super-SFD targets, respectively.

Power injection through the CEI is 30 MW, split evenly between ion and electron channels. Particle flux through the CEI is 1.9×10^{22} s^{-1}, representing both neutral beam particle input ($\Gamma_{NBI} = 4 \times 10^{21}$ s^{-1}) and auxiliary fueling. Ion and neutral recycling at simulated outer and PFR boundaries is set to 99% (except as noted below for the super-SFD), approximating the saturated walls of ST-FNSF in near-steady-state operation. Particle control is achieved via cryopumping, which is modeled by allowing neutral transmission through the surfaces indicated in Fig. 5. In the CD-VT case, transmission is 5%. In the other cases, transmission is 50%. Target recycling is 100% for ions and neutrals. To model neutral baffling in the super-SFD extended leg, neutral recycling is set to 100% for the surfaces with $R > 2$ m. Perpendicular transport cofficients are like the NSTX-U coefficients, except that the thermal transport is scaled down by a factor of two—this corresponds to the reduction in SOL heat flux width predicted by the heuristic drift-based model [17]. Nitrogen is included as a seeded impurity at 4% fixed concentration, and no intrinsic (sputtered) impurity is included. Gas power loss to the targets is included as in the NSTX-U cases. Gradient scale length boundary conditions are used for temperatures and densities at outer and PFR boundaries, with scale lengths set to 5 cm. Plasma drifts are not included.

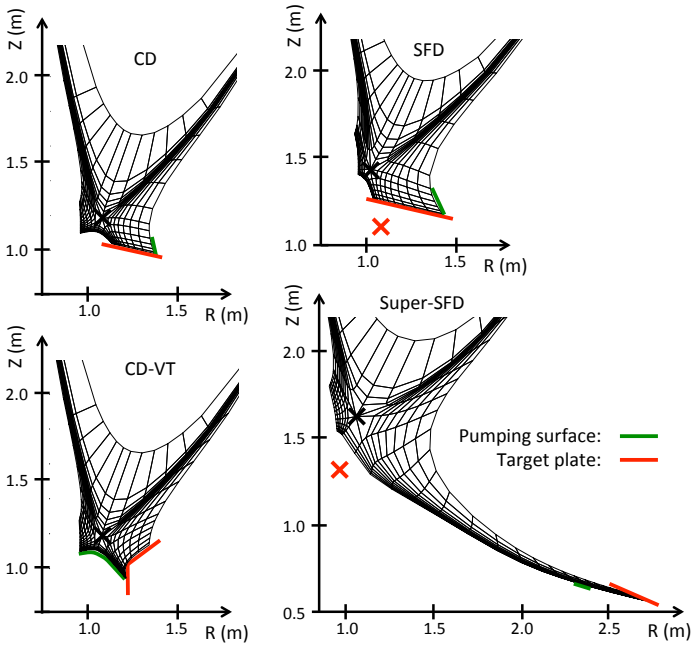

FIG. 5: ST-FNSF grids. Primary and secondary (snowflake) X-points are shown with black and red X's, respectively. Divertor cryopump surfaces and targets are indicated.

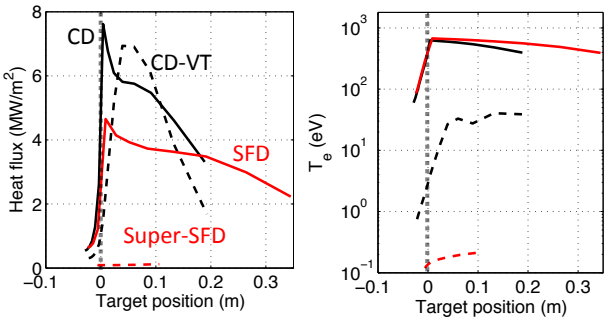

FIG. 6: ST-FNSF outer target heat fluxes and temperatures.

Results and discussion. Figure 6 shows outer target and midplane profiles for the ST-FNSF cases. In the CD and SFD cases, deposited heat fluxes are <10 MW/m^2, but unfavorable target tilt results in sheath-limited divertor plasmas, with target T_e within 10% of upstream T_e. In these cases, target T_e is in excess of 600 eV, which is unacceptable from a sputtering point of view, especially if the targets are composed of high-Z material. Notably, CD and SFD simulations with less target tilt (horizontal targets) yield

conduction-limited target plasmas with heat fluxes exceeding 20 MW/m^2. With improved neutral confinement, CD-VT and super-SFD cases have $T_e < 10$ eV near the OSP, and outer target heat fluxes < 10 MW/m^2. In the CD-VT, high outer target density is achieved through tilt-induced transport. For the super-SFD, however, tilt-induced transport is irrelevant—neutrals naturally accumulate in the closed end of the long leg, and the detachment front is localized near the cryopump duct. This behavior is analogous to water accumulating in a reservoir (the closed divertor leg) and eventually overflowing (into the cryopump duct). Super-SFD simulations with no target tilt yield similar full detachment. For all cases, inner target conditions are generally milder than outer target conditions, with lower T_e and heat flux; inner and outer SOL are disconnected, and three times more power is exhausted to the outer SOL than the inner SOL.

Of the 30 MW input power, only 2% is radiated by nitrogen in the CD and SFD cases. In the super-SFD and CD-VT cases, 37% and 25% of the input power is radiated by nitrogen. The reason for this disparity is that the radiative cooling rate (in W·m^3) for nitrogen peaks near 12 eV, and drops dramatically for higher temperatures. The CD and SFD are too hot to for nitrogen to act as a radiator. Impurities that radiate strongly at high temperatures (e.g., several hundred eV) can be detrimental to core confinement; thus, it is preferable to identify divertor configurations, like the super-SFD and CD-VT, that enable engagement of low-temperature radiators.

Note that the SFD here are "quasi-snowflakes" in the sense that the inter-X-point distance exceeds the heat flux width mapped to the primary X-point position. The near-target expansion in the SFD case provides the expected geometric heat flux reduction. In the super-SFD, though, the secondary X-point is far from the outer target, and probably has a minor effect on the UEDGE results.

4 Conclusions

Prior UEDGE modeling of the NSTX-U SFD [10] indicated that SFD divertor optimization should be considered to achieve favorable neutral confinement and thus avoid sheath-limited outer target plasma conditions. In pursuit of such optimization, several different SFD configurations are studied and compared. In SFD cases A, B, C, and D, the secondary X-point is translated horizontally across the outer target. Modeling of the four SFD cases and a conventional divertor case shows that SFD-C and -D configurations enable highly radiating, partially detached divertor conditions at relatively low core densities, and also provide a gradual detachment as core density is increased. This favorable result is attributed to improved neutral confinement as flux surfaces are tilted with respect to the target in SFD-C and -D.

Preliminary modeling of ST-FNSF divertor configurations indicate that control of neutral behavior is crucial to achieving low target temperature compatible with low sputtering yields. By managing neutral behavior with target tilt (CD-VT) or extension of the outer divertor leg (super-SFD), acceptable target temperatures (<50 eV) are achieved. In the CD-VT, neutrals are directed toward the outer strike point, promoting outer strike point detachment ($T_e \approx 2$ eV). In the super-SFD, full outer target detachment is seen, with the upstream cryopump duct providing natural detachment front stabilization.

This research provides guidance for upcoming experiments and a basis for continued development of predictive capability for divertor performance in STs. Numerous avenues remain to be explored in future ST divertor and SOL modeling. The UEDGE neutral model is limited to

flux-aligned grids similar to those presented here, but Monte Carlo neutral codes with greater flexibility are available, e.g., through the SOLPS package [18]. More flexible neutral modeling can more accurately represent geometric features such as neutral baffling and cryopump ducts. Charge-state-resolved impurity modeling should be developed and validated for the H-mode ST. As discussed in [8], the inclusion of drift phyics might be necessary to capture, even qualitatively, impurity transport behavior. Finally, several snowflake effects, such as instability-driven mixing in the region of weak poloidal field [19], are not included in this UEDGE modeling, and might play an important role.

5 Acknowledgments

Discussions with LLNL scientists D.D. Ryutov, M.V. Umansky, M.E. Rensink, and G.D. Porter, about divertor and snowflake physics, and about UEDGE, have been much appreciated. Special thanks also to D.A. Gates and F.M. Poli of PPPL, who provided valuable advice for running ISOLVER. This work was performed under the auspices of the U.S. Department of Energy by Lawrence Livermore National Laboratory under Contracts DE-AC52-07NA27344 and DE-AC02-09CH11466. This material is based upon work supported by the U.S. Department of Energy, Office of Science, Office of Fusion Energy Sciences. LLNL-PROC-661039

References

[1] MENARD, J. E. et al., Nucl. Fusion **51** (2011) 103014.
[2] RYUTOV, D. D., Phys. Plasmas **14** (2007) 064502.
[3] MENARD, J. E. et al., Nucl. Fusion **52** (2012) 083015.
[4] LOARTE, A. et al., Nucl. Fusion **47** (2007) S203.
[5] ROGNLIEN, T. D. et al., J. Nucl. Mater. **196** (1992) 347 .
[6] ROGNLIEN, T. D. et al., Fusion Eng. Design **60** (2002) 497 .
[7] SOUKHANOVSKII, V. A. et al., Phys. Plasmas **19** (2012) 082504.
[8] MEIER, E. T. et al., J. Nucl. Mater. (2015), Submitted.
[9] GRAY, T. K. et al., J. Nucl. Mater. **415** (2011) S360 .
[10] MEIER, E. T. et al., Contrib. Plasma Phys. **54** (2014) 454.
[11] HUANG, J. et al., U.S. Department of Energy Journal of Undergraduate Research (2005).
[12] HUTCHINSON, I. H., Nucl. Fusion **34** (1994) 1337.
[13] MCLEAN, A. G. et al., J. Nucl. Mater. (2015), Submitted.
[14] SCOTTI, F., PhD thesis, Princeton University, 2014.
[15] VALANJU, P. M. et al., Phys. Plasmas **16** (2009) 056110.
[16] HAVLICKOVA, E. et al., Plasma Phys. and Contr. Fusion **56** (2014) 075008.
[17] GOLDSTON, R. J., Nucl. Fusion **52** (2012) 013009.
[18] SCHNEIDER, R. et al., Contrib. Plasma Phys. **46** (2006) 3.
[19] RYUTOV, D. D. et al., Plasma Phys. Contr. Fusion **54** (2012) 124050.